

# The Star Formation History in the Andromeda Halo

By THOMAS M. BROWN

Space Telescope Science Institute, 3700 San Martin Drive, Baltimore, MD 21218

I present the preliminary results of a program to measure the star formation history in the halo of the Andromeda galaxy. Using the Advanced Camera for Surveys (ACS) on the Hubble Space Telescope, we obtained the deepest optical images of the sky to date, in a field on the southeast minor axis of Andromeda,  $51'$  (11 kpc) from the nucleus. The resulting color-magnitude diagram (CMD) contains approximately 300,000 stars and extends more than 1.5 mag below the main sequence turnoff, with 50% completeness at  $V = 30.7$  mag. We interpret this CMD using comparisons to ACS observations of five Galactic globular clusters through the same filters, and through  $\chi^2$ -fitting to a finely-spaced grid of calibrated stellar population models. We find evidence for a major ( $\sim 30\%$ ) intermediate-age (6–8 Gyr) metal-rich ( $[\text{Fe}/\text{H}] > -0.5$ ) population in the Andromeda halo, along with a significant old metal-poor population akin to that in the Milky Way halo. The large spread in ages suggests that the Andromeda halo formed as a result of a more violent merging history than that in our own Milky Way.

---

## 1. Introduction

One of the primary quests of observational astronomy is understanding the formation history of galaxies. An impediment to this research is the relative paucity of galaxies in the Local Group, which contains no giant ellipticals, and only two giant spirals – our own Milky Way and Andromeda. Fortunately, Andromeda (M31, NGC224) is well-situated for studying the formation of giant spiral halos, due to its proximity (770 kpc; Freedman & Madore 1990), small foreground reddening ( $E_{B-V} = 0.08$  mag; Schlegel, Finkbeiner, & Davis 1990), and low inclination ( $i \approx 12.5^\circ$ ; de Vaucouleurs 1958). Andromeda is similar to the Milky Way in many respects (Hubble type, absolute magnitude, mass, and size; van den Bergh 1992; Klypin, Zhao, & Somerville 2002), but we have long known that its halo is more metal-rich than that of the Milky Way; the metallicity distribution in the Milky Way halo peaks near  $[\text{Fe}/\text{H}] \approx -1.8$  (Ryan & Norris 1991), while that in the Andromeda halo peaks near  $[\text{Fe}/\text{H}] \approx -0.5$  (Mould & Kristian 1986; Holland, Fahlman, & Richer 1996; Durrell, Harris, & Pritchett 2001). Although the Milky Way halo is dominated by old stars (e.g., VandenBerg 2000), the formation history of the Andromeda halo has been unknown until now.

Physical processes possibly at work in forming spiral halos include rapid dissipative collapse in the early universe (Eggen, Lynden-Bell, & Sandage 1962), slower accretion of separate subclumps (Larson 1969; Searle & Zinn 1978), and dissolution of globular clusters (Aguilar, Hut, & Ostriker 1988). More recent hierarchical models suggest that spheroids (bulges and halos) form in a repetitive process during the mergers of galaxies and protogalaxies, while disks form by slow accretion of gas between merging events (e.g., White & Frenk 1991). The discovery of the Sgr dwarf galaxy (Ibata, Gilmore, & Irwin 1994) sparked renewed interest in halo formation through accretion of dwarf galaxies, and ambitious programs are now underway to map out the spatial distribution, kinematics, and chemical abundance in the halos of the Milky Way (e.g., Morrison et al. 2000; Majewski et al. 2000) and Andromeda (e.g., Ferguson et al. 2002). In the meantime, the realization that hierarchical models based on cold dark matter almost inevitably predict many more dwarf galaxies than are actually seen around the Milky Way (Moore et al. 1999)

has led to suggestions that most of the dwarf galaxies formed in the early Universe have dissolved into the halo (e.g., Bullock, Kravtsov, & Weinberg 2000). Whether or not such accretion is the dominant source of stars in the stellar halo, it is likely that dwarf galaxies do contribute, and at large galactocentric distances their stars can remain in coherent orbital streams for many Gyr. Indeed, one such stream has been found in the halo of Andromeda (Ibata et al. 2001; McConnachie et al. 2003); Ferguson et al. (2002) demonstrated dramatic evidence for large-scale debris trails and substructure in the M31 halo and outer disk, yet their deep imaging and star counts also found an apparently smooth component extending to large radii.

The most direct way to measure ages in a stellar population is to construct a color-magnitude diagram (CMD) that reaches to stars below the main sequence turnoff. For decades, researchers have used such data to determine the ages of Galactic globular clusters and satellite galaxies of the Milky Way, but until now there has been no instrument capable of resolving these stars in a massive galaxy outside of our own. With the installation of the Advanced Camera for Surveys (ACS; Ford et al. 1998) on the Hubble Space Telescope (HST), this is now possible. We have obtained deep ACS observations of a minor axis field in Andromeda's halo,  $\approx 51$  arcmin (11 kpc) from the nucleus. In these proceedings, I present the preliminary results of our program (Brown et al. 2003). I start with a brief review of the age diagnostics available in a deep CMD, then describe our ACS observations and their analysis, and finish with the implications for the formation history of Andromeda.

## 2. Age Diagnostics

Stellar population ages are best determined from resolved optical photometry reaching the main sequence. Although the location of the main sequence turnoff in the CMD is the primary age indicator, photometry reaching well below the turnoff is required to define the turnoff accurately. Ages among the Galactic globular clusters are usually determined via one of two diagnostics (figure 1): the luminosity difference between the turnoff and the horizontal branch (Sandage 1982; Iben & Renzini 1984), and the color difference between the turnoff and the red giant branch (VandenBerg, Bolte, & Stetson 1990). The luminosity of the horizontal branch and the color of the red giant branch are both relatively insensitive to age (at fixed composition), while the main sequence turnoff becomes both fainter and redder at increasing age. Our ACS observations used the F606W (broad  $V$ ) and F814W ( $I$ ) filters; for roughly every Gyr beyond 10 Gyr, the main sequence turnoff becomes fainter by  $\sim 0.1$  mag in  $m_{F814W}$  and redder by  $\sim 0.01$  mag in  $m_{F606W} - m_{F814W}$  (see figure 1).

The age-metallicity degeneracy is a major uncertainty when characterizing individual stars via photometry, or unresolved populations via low-resolution spectra (figure 2a). However, the situation is better for a resolved stellar population. Because the red giant branch is much more sensitive to metallicity than age, and the subgiant branch and main sequence turnoff are sensitive to both age and metallicity, the distribution of stars on the red giant branch, subgiant branch, and main sequence turnoff can be simultaneously reproduced only for specific combinations of age and metallicity (figure 2).

## 3. Observations

Using the ACS Wide Field Camera (WFC), we obtained deep optical images of a field along the southeast minor axis of the M31 halo, at  $\alpha_{2000} = 00^h 46^m 07^s$ ,  $\delta_{2000} = 40^\circ 42' 34''$  (figure 3). The field was previously imaged by Holland et al. (1996) with the Wide Field

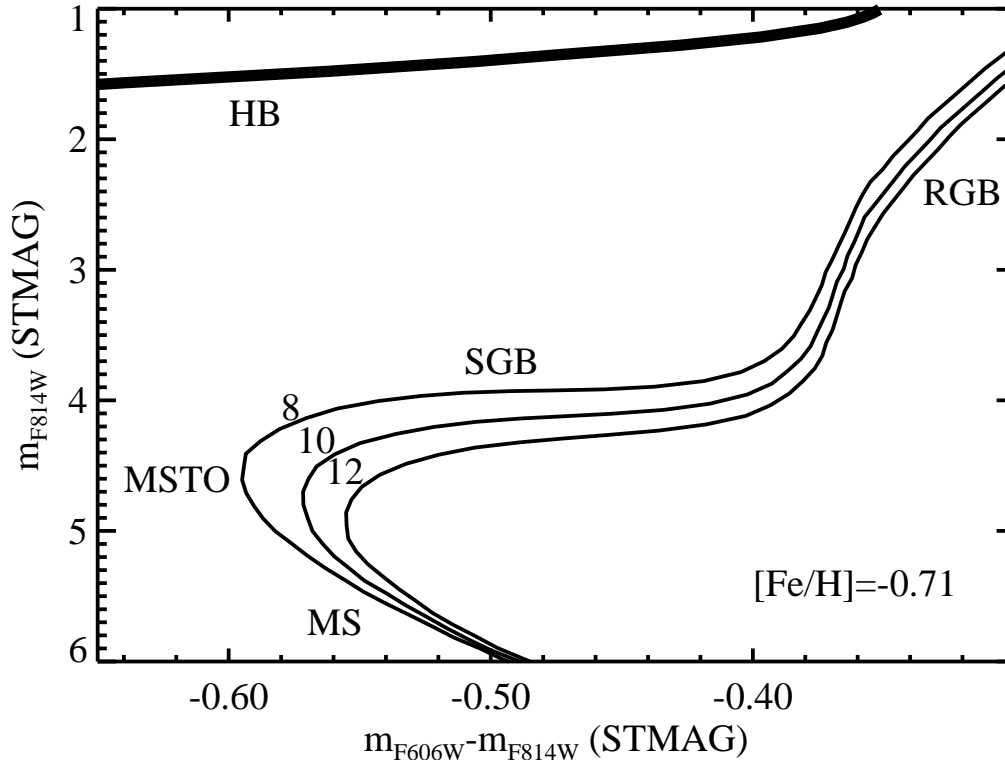


FIGURE 1. The variation in optical photometry of a stellar population with age at fixed metallicity (*labeled*). Isochrones at 8, 10, and 12 Gyr (*labeled*) are shown in a CMD constructed using the ACS bandpasses F606W and F814W. Note that the subgiant branch (SGB) and main sequence turnoff (MSTO) are more sensitive to age than the red giant branch (RGB). The primary age indicators in the CMD are the luminosity difference between the MSTO and the horizontal branch (HB), which becomes larger as age increases, and the color difference between the MSTO and the RGB, which becomes smaller as age increases. However, in order to clearly define the MSTO, photometry must extend to the main sequence (MS) stars below the MSTO.

Planetary Camera 2 (WFPC2); the field is not associated with the tidal streams and substructure found by Ferguson et al. (2002), and lies just outside the “flattened inner halo” in their maps. Given the nearly edge-on disk, the contribution of disk stars at this position should be  $\lesssim 3\%$  (Walterbos & Kennicutt 1988; Holland et al. 1996 and references therein). We chose this field to optimize the crowding (trading off population statistics versus photometric accuracy) and to place an interesting M31 globular cluster (GC312; Sargent et al. 1977) near the edge of our images. The metallicity of GC312 ( $[\text{Fe}/\text{H}] = -0.7$ ; Huchra, Brodie, & Kent 1991) is near the peak in the metallicity distribution for the M31 halo; this should simplify our attempts to derive relative ages for this cluster and the halo (currently underway). Due to scheduling and orientation constraints, one bright foreground star ( $V \sim 14$  mag) was unavoidable; the star and its window reflection affect a few percent of the total image area, which we discard.

From 2 Dec 2002 to 11 Jan 2003, we obtained 39.1 hours of ACS images in the F606W filter (broad  $V$ ) and 45.4 hours in the F814W filter ( $I$ ), with every exposure dithered to allow for hot pixel removal, optimal sampling of the point spread function, smoothing of the spatial variations in the detector response, and filling the gap between the two halves of the  $4096 \times 4096$  pix detector. We co-added the M31 images using the IRAF DRIZZLE

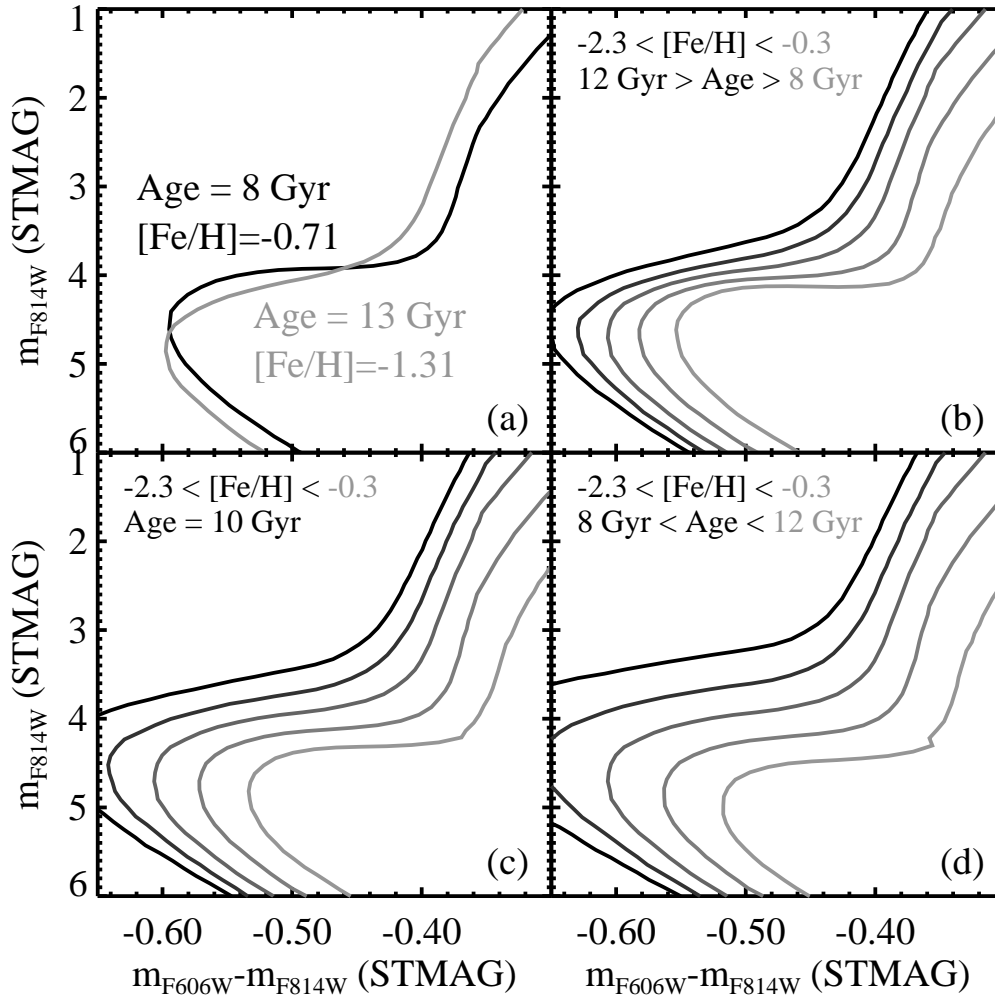


FIGURE 2. *Panel a:* An isochrone of intermediate age and metallicity (*dark curve, labeled*) and an older, more metal-poor isochrone (*light curve, labeled*) intersect, demonstrating that two-color photometry for a single star does not uniquely determine age and metallicity. Both isochrones also have the same color at the main sequence turnoff, and thus unresolved populations with these parameters would appear very similar. However, resolved photometry could distinguish between two such populations. *Panel b:* Isochrones spanning 8-12 Gyr at 1 Gyr intervals, with a range in metallicity (*labeled*) anticorrelated with age, such that the youngest isochrone is the most metal-rich, as might be expected for a simple model of chemical evolution. The subgiant branch and main sequence turnoff both become fainter and redder at increasing age or increasing metallicity, while the red giant branch is more sensitive to metallicity than age. Because the effects of age and metallicity counteract each other at the subgiant branch, it appears very narrow compared to the red giant branch. *Panel c:* The same metallicities as in *b*, but all of the isochrones have the same age. *Panel d:* The same metallicities and ages as in *b*, but now age is correlated with metallicity, such that the older populations are more metal-rich. This is somewhat unphysical, but demonstrates a situation of renewed star formation from the infall of primordial gas. Note the width of the subgiant branch compared to the red giant branch. Panels *b-d* demonstrate that resolved photometry of a mixed population can disentangle age and metallicity, because each evolutionary phase responds differently to these parameters.

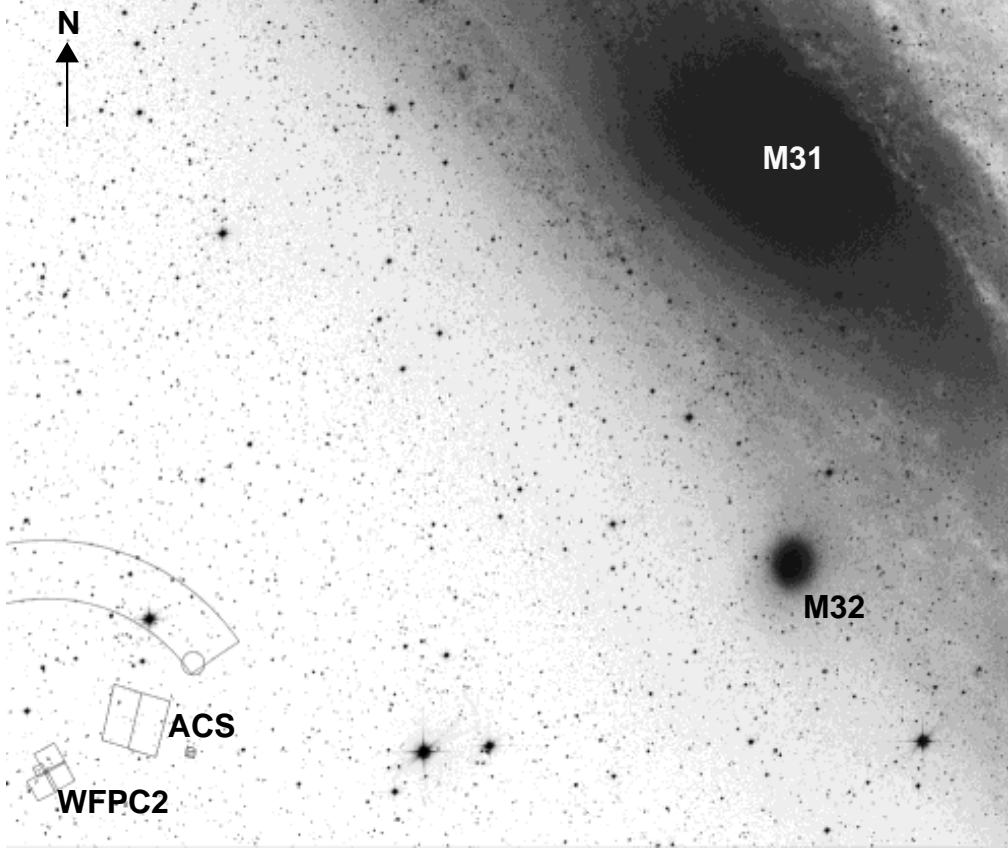


FIGURE 3. A  $50' \times 60'$  Digital Sky Survey image of Andromeda, showing the positions of our ACS and WFPC2 images (labeled). The ACS field is 50 arcmin (11 kpc) from the center of M31. The nearly edge-on ( $i \approx 12.5^\circ$ ; de Vaucouleurs 1958) disk should contribute  $\lesssim 3\%$  of the stars in the ACS field.

package, with masks for the cosmic rays and hot pixels, resulting in geometrically-correct images with a plate scale of  $0.03'' \text{ pixel}^{-1}$  and an area of approximately  $210'' \times 220''$  (figure 4). We then performed both aperture and PSF-fitting photometry using the DAOPHOT-II package (Stetson 1987), assuming a variable PSF constructed from the most isolated stars in the images. The aperture photometry on isolated stars was corrected to true apparent magnitudes using TinyTim models of the HST PSF (Krist 1995) and observations of the standard star EGGR 102 (a  $V = 12.8$  mag DA white dwarf) in the same filters, with agreement at the 1% level. The PSF-fitting photometry was then compared to the corrected aperture photometry, in order to derive the offset between the PSF-fitting photometry and true apparent magnitudes. Our photometry is in the STMAG system:  $m = -2.5 \times \log_{10} f_\lambda - 21.1$ . For those more familiar with the Johnson  $V$  and Cousins  $I$  bandpasses, a 5,000 K stellar spectrum has  $V - m_{F606W} = -0.05$  mag and  $I - m_{F814W} = -1.28$  mag.

Of the  $\sim 300,000$  stars detected, we discarded those within the GC312 tidal radius ( $10''$ ; Holland, Fahlman, & Richer 1997), within  $14.5''$  of a bright foreground star, within  $12.6''$  of this star's window reflection, and near the image edges, leaving  $\approx 223,000$  stars in the final catalog. Using the SExtractor code (Bertin & Arnouts 1996), we estimate  $\lesssim 5\%$

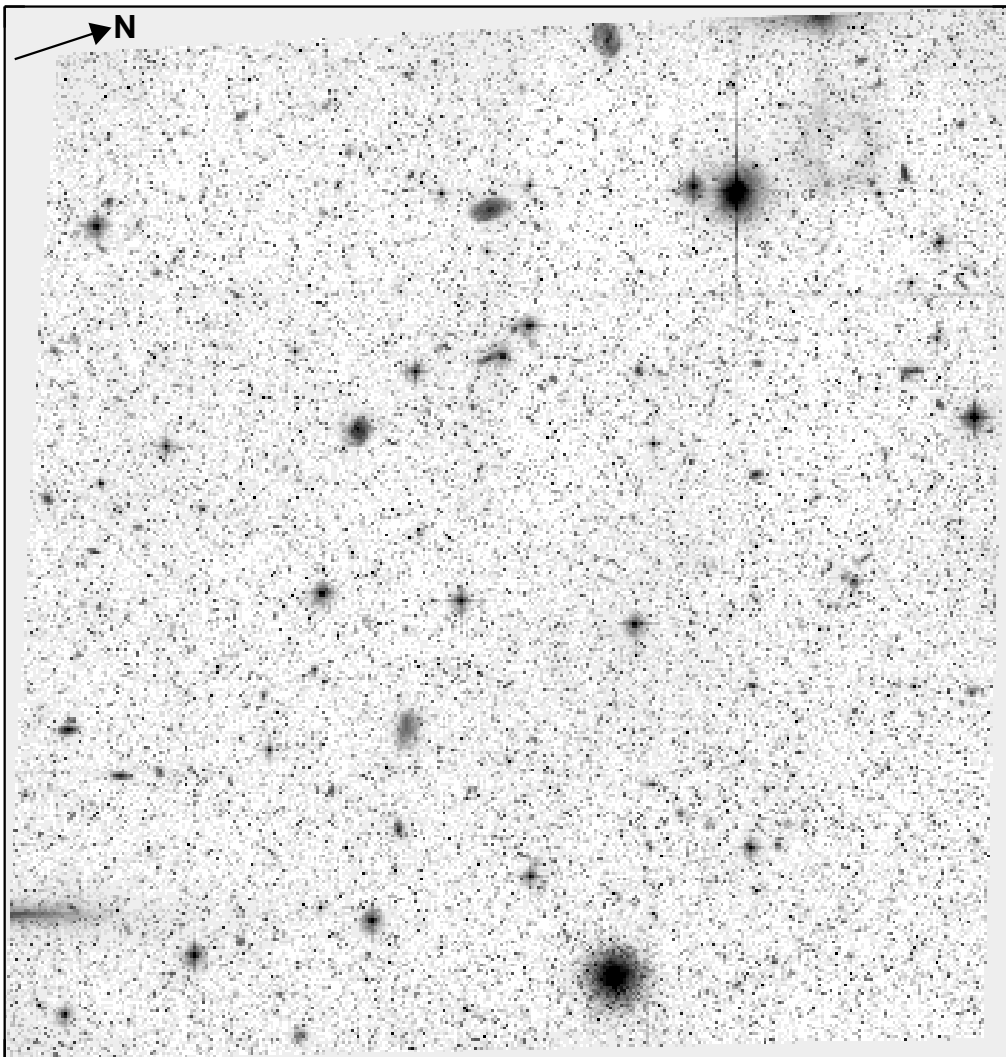


FIGURE 4. The ACS F606W image of the Andromeda halo, shown at a log stretch, and binned for display purposes by a factor of 20, to  $0.6'' \text{ pixel}^{-1}$ . The field subtends  $211'' \times 221''$  (not much larger than the WFC field of view, because the largest dither was about  $6''$ ). For our preliminary analysis, we excluded the area around GC312 (*bottom*) and around a bright ( $V = 14 \text{ mag}$ ) foreground star (*upper right*) and its window reflection (to the right of the star). Many background galaxies can be seen through the 300,000 stars detected in Andromeda's halo, but they are a small ( $< 5\%$ ) contamination. The image has been corrected for the strong geometric distortion in the camera, giving the field its unusual shape.

of the stars are contaminated by extended sources (figure 5). Extensive artificial star tests determine the photometric scatter and completeness as a function of color and luminosity. The CMD shows no obvious differences when comparing the population in a  $10\text{--}100''$  annulus around GC312 to that beyond  $100''$ ; the cluster does not appear to be associated with an extended underlying system. By integrating our catalog, we estimate that the surface brightness in our field is  $\mu_V \approx 26.3 \text{ mag arcsec}^{-2}$ .

We also obtained coordinated parallel WFPC2 observations of a second field along the minor axis of Andromeda (figure 3) using the same bandpasses as those in the ACS

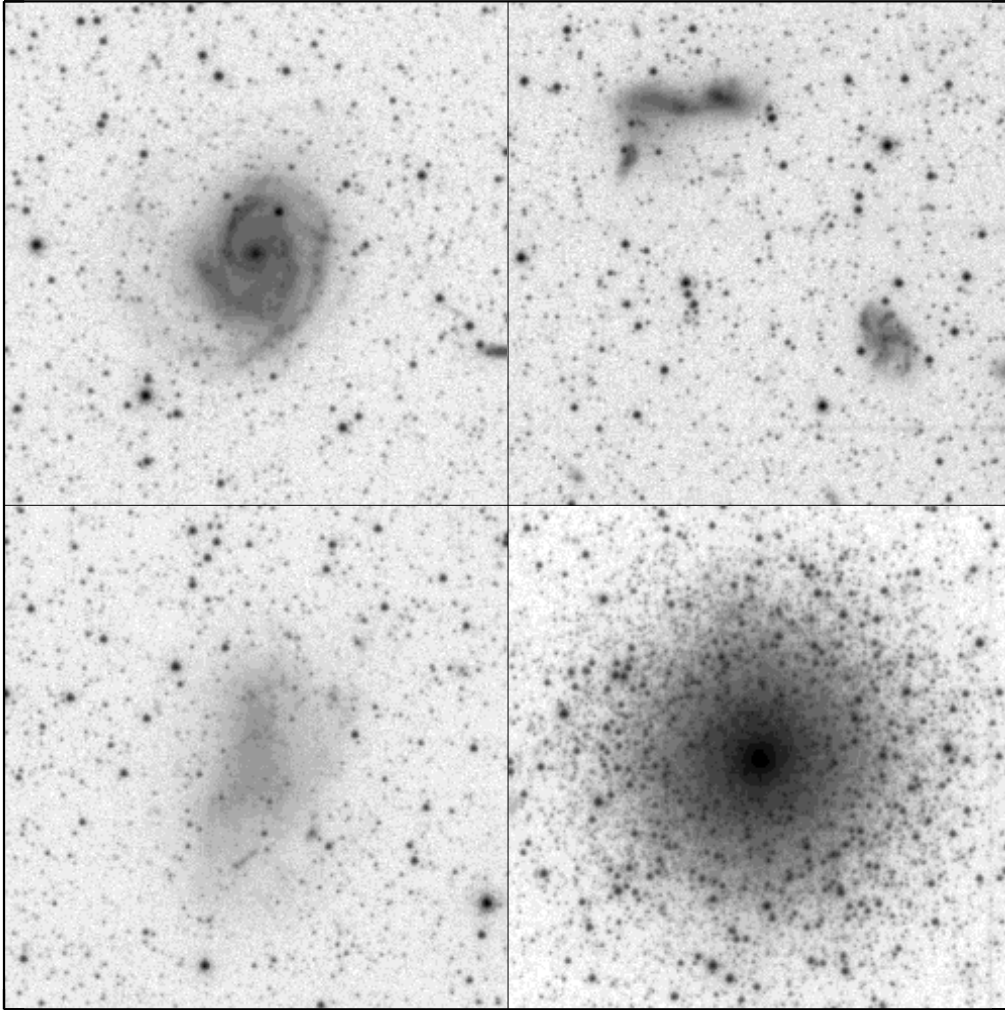


FIGURE 5. Subsections ( $15'' \times 15''$ ) of the ACS image show the globular cluster GC312 in Andromeda's halo (*lower right*), background galaxies, and the level of crowding in the halo population. The images have been rebinned to a scale of  $0.06'' \text{ pixel}^{-1}$  for display purposes.

observations. The WFPC2 data are not nearly as deep as the ACS data, but they are about as deep as the Hubble Deep Field (Williams et al. 1996), and thus much deeper than any Andromeda observations prior to our program. Although the WFPC2 images resolve stars at the main sequence turnoff, the resulting CMD is not deep enough to characterize the turnoff and subgiant branch well. The striking differences between the WFPC2 and ACS CMDs are a testament to the technical advances achieved by the HST servicing missions (figure 6).

Because the ACS is a new instrument, our program includes ACS observations of five Galactic globular clusters spanning a wide metallicity range (Table 1), using the same filters utilized in our Andromeda halo observations. These cluster images allow the construction of empirical isochrones in the ACS bandpasses, which can be directly compared to the Andromeda CMD and used to calibrate the transformation of the theoretical isochrones to the ACS bandpasses. Figure 7 shows the ACS F606W image

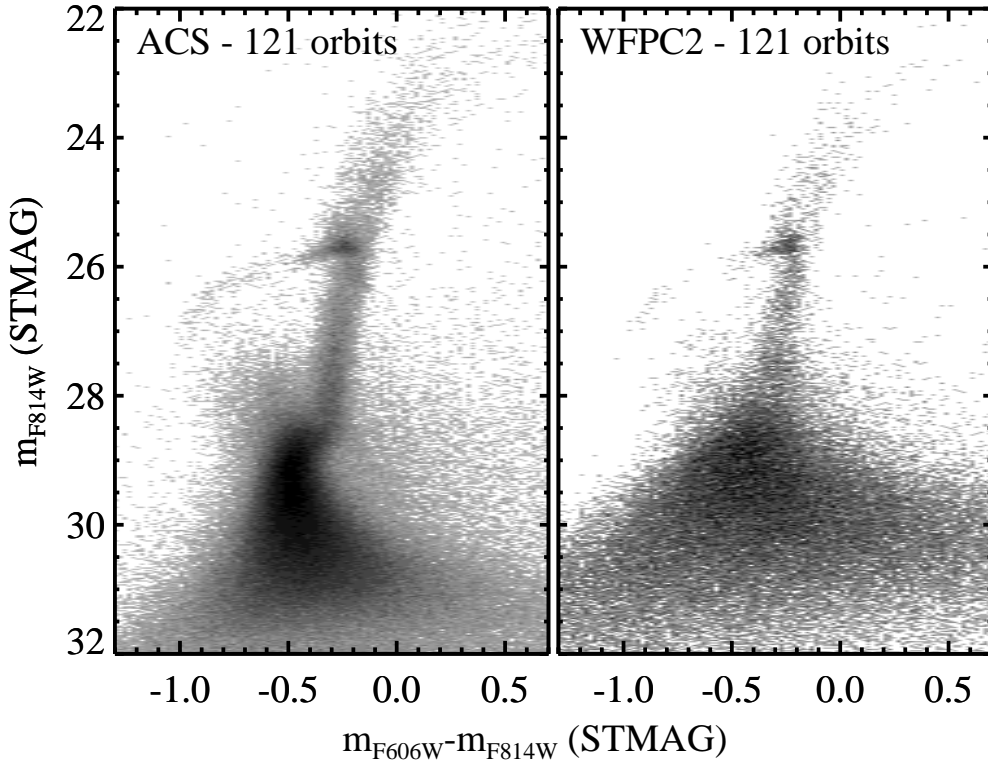


FIGURE 6. *Left panel:* The CMD constructed from the ACS images of the Andromeda halo, using aperture photometry. There are too many stars to plot them individually; instead, this is a Hess diagram at a logarithmic stretch. *Right panel:* The CMD constructed from the parallel WFPC2 images, in a field a few arcmin further out along the minor axis of Andromeda, again using aperture photometry. The filters and exposure times in the WFPC2 data are approximately the same as those in the ACS data. Although the WFPC2 data reach stars at the main sequence turnoff, they are not deep enough to characterize the subgiant branch and the turnoff well.

of M92. M92, NGC6752, and 47 Tuc are the most useful calibrators in our program, because their parameters are known very well; NGC5927 and NGC6528 are also useful because of their high metallicities, but their parameters are less secure, and they suffer from high, spatially variable foreground reddening (Heitsch & Richtler 1999). To increase the dynamic range, three images were taken in each bandpass for each cluster, with the exposure times varying by an order of magnitude. To minimize the number of orbits required for the cluster data, these observations were not dithered. Thus, we drizzled the data without plate scale changes, in order to remove cosmic rays and to correct for geometric distortion. The cluster images are significantly less crowded (on average) than those of M31, and the  $0.05''$  pixels undersample the PSF, so we performed aperture photometry but no PSF fitting, and corrected the aperture photometry to true apparent magnitudes (figure 8).

#### 4. Analysis

The ACS CMD reveals, for the first time, the main sequence population in the M31 halo. The horizontal branch extends from a well-populated red clump to a minority blue population ( $\sim 10\%$  of the total horizontal branch population). The horizontal branch is

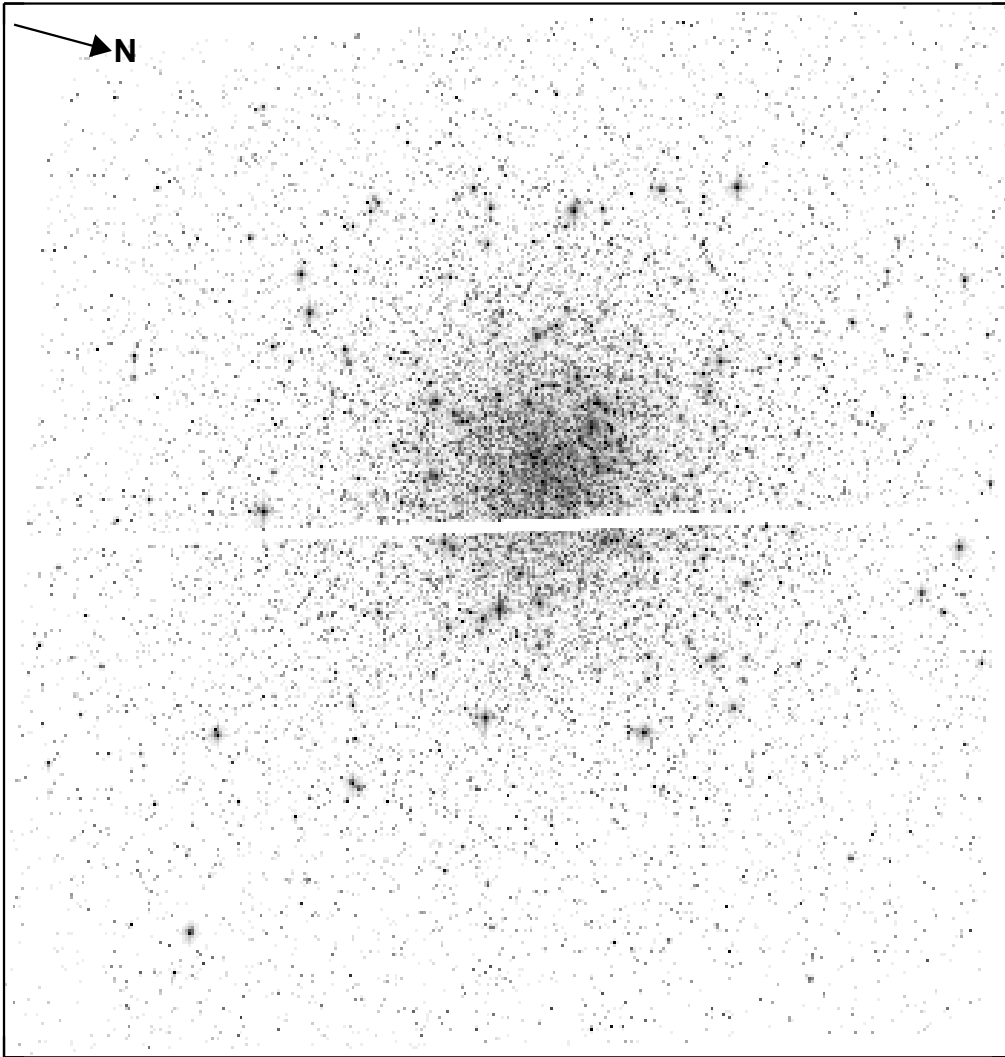


FIGURE 7. The ACS F606W image of M92, shown at a log stretch and binned by 20 to  $0.6''$   $\text{pixel}^{-1}$  for display purposes. The globular cluster images in our program were not dithered, so a gap appears between the two WFC chips.

not noticeably extended – the hot horizontal branch stars that are seen in clusters like NGC6752 are missing. The broad red giant branch indicates a wide metallicity distribution extending to near-solar metallicities, long-known to be characteristic of the M31 halo (Mould & Kristian 1986). The luminosity function “bump” on the red giant branch is another metallicity indicator, becoming fainter as metallicity increases; it slopes away from the red horizontal branch until the luminosity difference reaches  $\approx 0.5$  mag – another indication of near-solar metallicities. There is also a prominent blue plume of stars significantly brighter than the main sequence turnoff; this minority population ( $\sim 2\%$  the size of the population at the turnoff  $\pm 1$  mag) may include binaries, blue stragglers, or a residual young stellar population. Although the blue horizontal branch stars are characteristic of very old, metal-poor globular clusters (such as M92), the luminosity difference between the turnoff and horizontal branch is smaller than expected for a purely old stellar

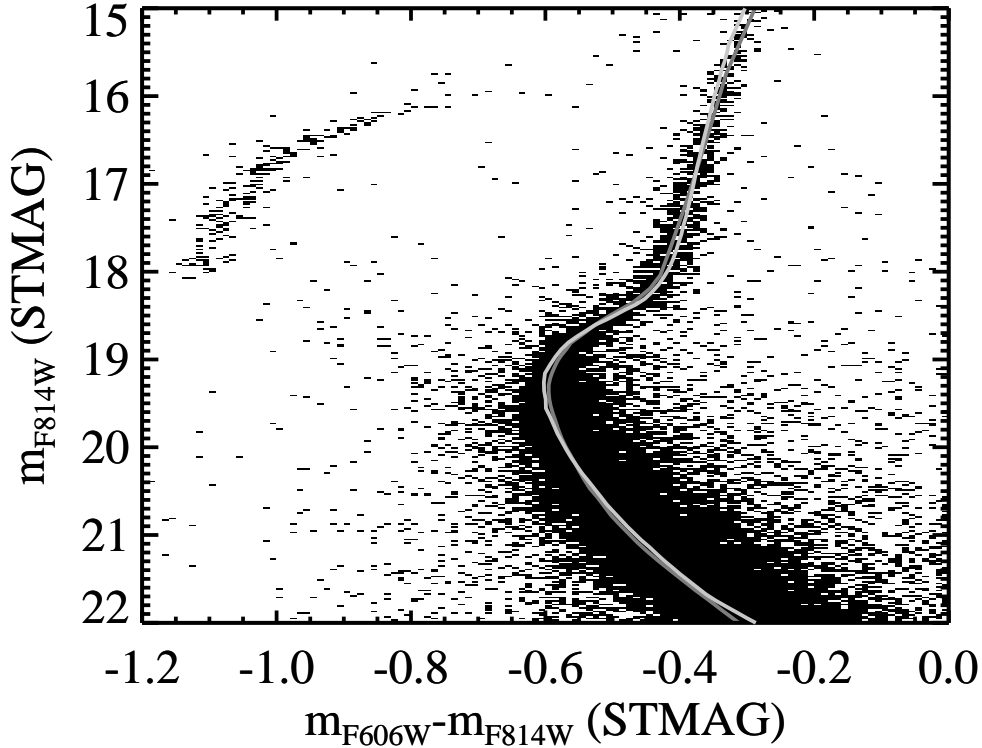


FIGURE 8. The CMD created from our ACS images of M92. The ridge line for this cluster (*dark grey curve*) was created by taking the median  $m_{F606W} - m_{F814W}$  color and median  $m_{F814W}$  for a series of points along the main sequence and red giant branch. A 14 Gyr isochrone at  $[\text{Fe}/\text{H}] = -2.14$  (*light grey curve*), transformed to the ACS bandpasses, agrees well with the ridge line over the CMD region used for fitting the Andromeda halo population.

population. This is shown in figure 9, which shows the ridge lines and horizontal branch loci for the five globular clusters we observed with ACS, superimposed upon the CMD of Andromeda. The M31 subgiant branch is nearly horizontal, indicating a high metallicity, while its ridge is appreciably brighter than those of 47 Tuc, NGC5927, and NGC6528, implying the presence of a significantly younger population in the M31 halo.

The comparison between the globular clusters and Andromeda in figure 9 provides a completely empirical indication of the age spread in Andromeda’s halo. M92, NGC6752, and 47 Tuc were shifted in color and magnitude according to the differences in reddening and distance between the clusters and Andromeda. Those shifts naturally aligned the horizontal branch loci of these clusters to the horizontal branch of Andromeda, thus demonstrating the accuracy of the parameters in Table 1, but we could have simply aligned the horizontal branches without any knowledge of the relative distances and reddenings. Indeed, forcing alignment at the horizontal branch was required for NGC5927 and NGC6528, because the parameters of those clusters are very uncertain. Once the clusters are all aligned at the horizontal branch, the red giant branches of the clusters span the broad red giant branch of Andromeda, empirically demonstrating the wide metallicity distribution in Andromeda’s halo. For the most metal-poor cluster (M92; *lightest grey curve* in figure 9), the subgiant branch luminosity agrees well with that in Andromeda, and the turnoff of the cluster agrees well with the blue edge of the turnoff in Andromeda; this indicates that Andromeda contains a significant population of metal-

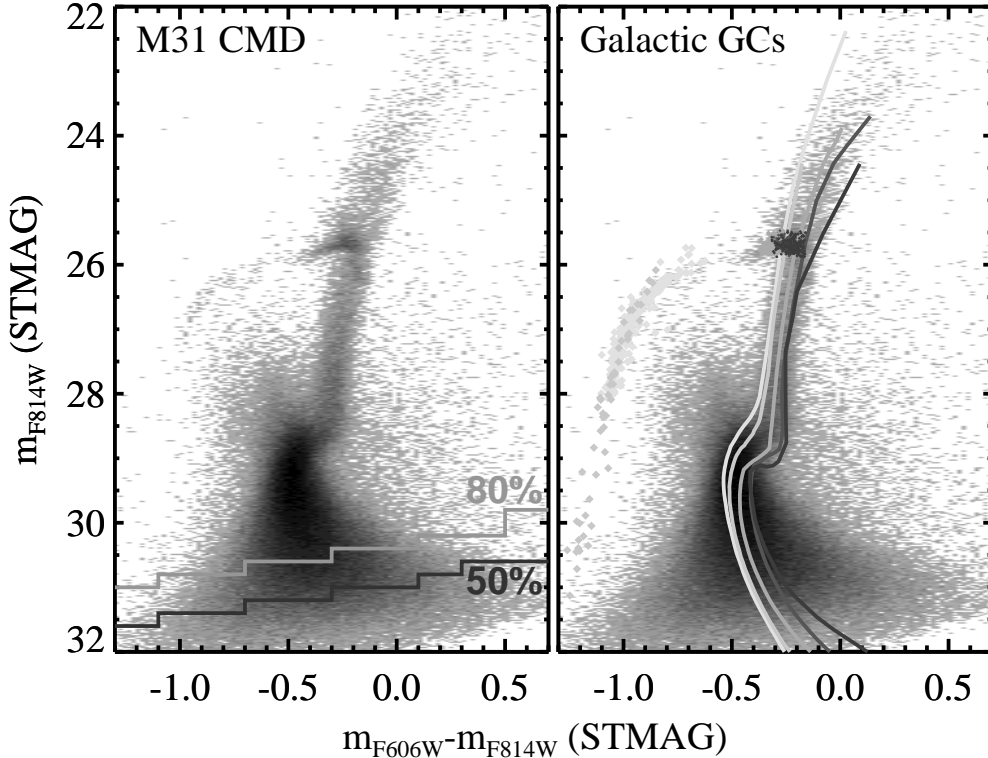


FIGURE 9. *Left panel:* The CMD of Andromeda constructed from the PSF-fitting photometry of the ACS images. Completeness limits determined from artificial star tests are marked. *Right panel:* The CMD of Andromeda, with the ridge lines (*grey curves*) and horizontal branch loci (*grey diamonds*) of five Galactic globular clusters superimposed. The shading of the ridge lines and horizontal branch points range from light grey to dark grey as the cluster metallicity increases (see Table 1). The data for M92, NGC6752, and 47 Tuc have only been shifted by the differences in distance and reddening between the clusters and M31, yet their horizontal branch loci agree well with the horizontal branch of M31. Those parameters are very uncertain for NGC6528 and NGC5927, so the data for the two metal-rich clusters were shifted to align their horizontal branch loci with the M31 horizontal branch: NGC6528 was shifted 0.16 mag brighter, while NGC5927 was shifted 0.11 mag brighter and 0.05 mag redder. Moving from the most metal-poor cluster (M92) to the most metal-rich (NGC6528), the red giant branches of the clusters span the width of the red giant branch in M31, yet the subgiant branches of the clusters become increasingly fainter than that of M31, indicating that the metal-rich stars in the M31 halo are much younger than those in the clusters.

poor stars with ages similar to the oldest Galactic globular clusters. However, as one compares clusters at increasing metallicity to Andromeda, discrepancies at the subgiant branch and turnoff become more apparent. Although the red giant branches of 47 Tuc, NGC5927, and NGC6528 straddle a large fraction of the red giant branch population in Andromeda, the cluster subgiant branches are well below the bulk of the subgiant population in Andromeda. This is a strong indication that the metal-rich populations in Andromeda are significantly younger than the cluster, given that the subgiant branch and turnoff become fainter by approximately 0.1 mag for every 1 Gyr increase in age.

Our full analysis of the star formation history is in progress. Here, I will supplement the comparisons shown in figure 9 with examples from the modeling to date (figure 10). Our modeling is based upon the isochrones of VandenBerg, Bergbusch, & Dowler (2003,

TABLE 1. M31 and globular cluster parameters

| Name<br>Name | $(m - M)_V$<br>(mag) | $E_{B-V}$<br>(mag) | [Fe/H]             | Exposure<br>(s) |        |
|--------------|----------------------|--------------------|--------------------|-----------------|--------|
|              |                      |                    |                    | F606W           | F814W  |
| M31          | 24.68 <sup>a</sup>   | 0.08 <sup>b</sup>  | -0.6 <sup>c</sup>  | 140870          | 163570 |
| M92          | 14.60 <sup>d</sup>   | 0.023 <sup>b</sup> | -2.14 <sup>d</sup> | 95.5            | 106.5  |
| NGC6752      | 13.17 <sup>e</sup>   | 0.055 <sup>b</sup> | -1.54 <sup>f</sup> | 44.5            | 49.5   |
| 47 Tuc       | 13.27 <sup>g</sup>   | 0.032 <sup>b</sup> | -0.83 <sup>f</sup> | 76.5            | 78     |
| NGC5927      | 15.81 <sup>h</sup>   | 0.45 <sup>h</sup>  | -0.37 <sup>h</sup> | 532             | 355.7  |
| NGC6528      | 16.15 <sup>i</sup>   | 0.55 <sup>i</sup>  | -0.2 <sup>i</sup>  | 504             | 371    |

<sup>a</sup>Freedman & Madore (1990). <sup>b</sup>Schlegel et al. (1998). <sup>c</sup>Mould & Kristian (1986). <sup>d</sup>VandenBerg & Clem (2003). <sup>e</sup>Renzini et al. (1996). <sup>f</sup>VandenBerg (2000). <sup>g</sup>Zoccali et al. (2001). <sup>h</sup>Harris (1996). <sup>i</sup>Momany et al. (2003).

in preparation), which show good agreement with cluster CMDs spanning a wide range of metallicity and age (e.g., figure 8). To transform these isochrones from the ground-based bandpasses to the HST-based bandpasses, we used the spectra of Lejeune, Cuisinier, & Buser (1997) to calculate  $V - m_{F606W}$  and  $I - m_{F814W}$ , as a function of effective temperature and gravity along the isochrones, then applied those differences to the ground-based magnitudes of the isochrones, with a small ( $\lesssim 0.05$  mag) empirical color correction to force agreement with our globular cluster CMDs. After this correction, the isochrones match the ridge lines within  $\lesssim 0.02$  mag over the region of the CMD we are fitting. Our observed CMDs of these clusters are reproduced by a 12.5 Gyr isochrone for 47 Tuc and 14 Gyr isochrones for NGC6752 and M92. The isochrones do not include core He diffusion, which would reduce their ages by 10–12%, thus avoiding discrepancies with the age of the Universe (VandenBerg et al. 2002).

Using isochrones with a range of ages and metallicities, we fit the region of the M31 CMD shown in figure 10a using the StarFish code of Harris & Zaritsky (2001). Restricting the fit to this region of the CMD focuses on the most sensitive age and metallicity indicators while avoiding regions of the CMD that are seriously incomplete, sparsely populated, or poorly constrained by the models (e.g., the horizontal branch morphology). Note that we do not include the red giant branch luminosity function bump in our fitting; although theory predicts that this bump becomes fainter with increasing metallicity, the theoretical zeropoint is fairly uncertain. The StarFish code fits the observed CMD through a linear combination of input isochrones, using  $\chi^2$  minimization, where the isochrones are scattered according to the results of the artificial star tests. We first followed the standard method used when researchers determine the metallicity distribution from the red giant branch (figure 10b). We fit the red giant branch using a set of old (13.5 Gyr) isochrones spanning a wide metallicity range ( $-2.31 < [\text{Fe}/\text{H}] < 0$ ). The resulting metallicity distribution was similar to that found by Holland et al. (1996) in our same field, and Durrell et al. (2001) in a field 20 kpc from the nucleus. However, it is very obvious that these purely old isochrones do not match the subgiant branch or the turnoff. Next, as shown in figure 10c, we tried fitting the entire region of figure 10a with a wider age range (11.5–13.5 Gyr), but found no acceptable combination. The insets

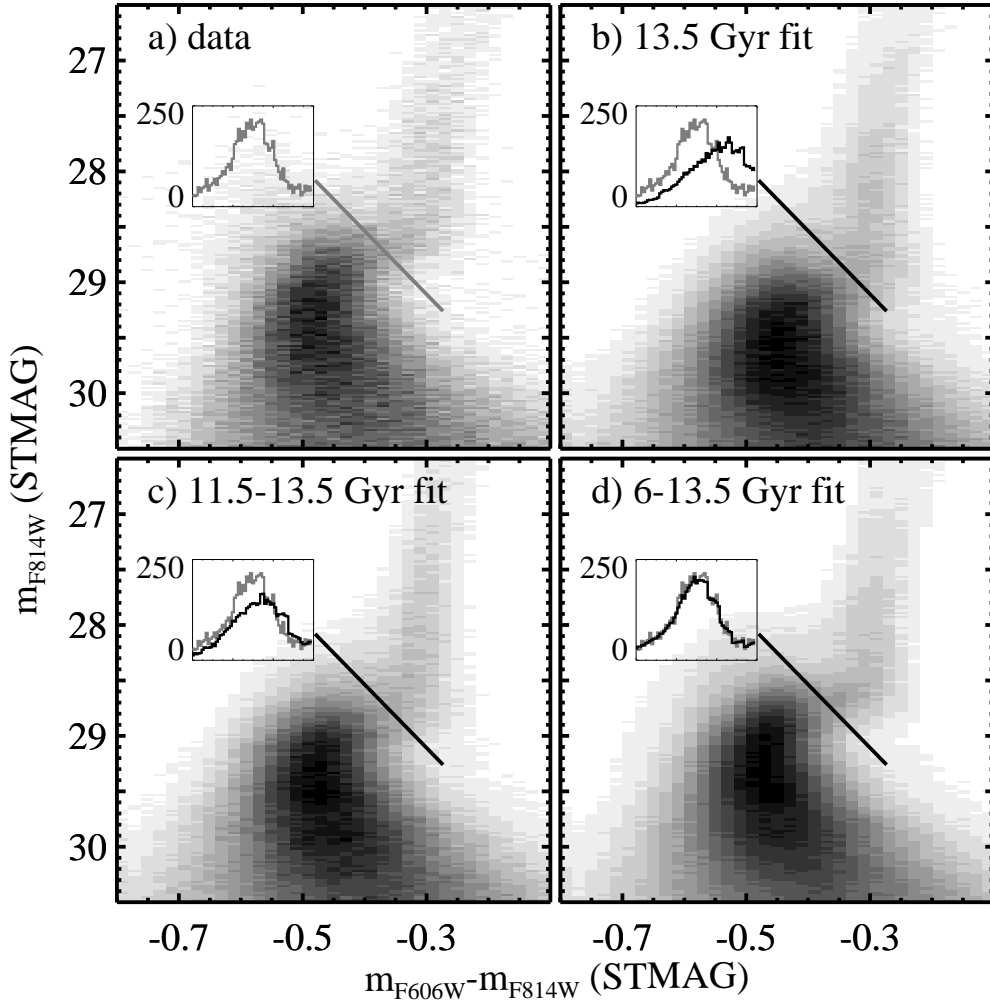


FIGURE 10. *Panel a*: The region of the Andromeda halo CMD that we used for fitting the star formation history. Restricting the fit to this region avoids parts of the CMD that are seriously incomplete, sparsely populated, or poorly constrained by the theoretical models. A histogram (*inset*) of the number of stars along a cut through the subgiant branch (*grey line*) highlights the differences between the data and the models in the subsequent panels. *Panel b*: The fit to the red giant branch using only 13.5 Gyr isochrones spanning a wide range in metallicity. Although such models can reproduce the width of the Andromeda red giant branch, the subgiant branch and turnoff are much fainter than those in the data. The histogram (*inset*) compares the number of stars along the cut (*black line*) through the subgiant branch to that in the data (*grey histogram*); they are poorly matched. *Panel c*: The fit to the entire region shown in panel *a*, using isochrones with a wide metallicity range but ages of 11.5–13.5 Gyr. The histogram (*inset*) again highlights that this model does not reproduce the distribution seen in the data. *Panel d*: The fit to the data shown in panel *a*, using a wide metallicity range and ages of 6–13.5 Gyr. This model reproduces the data well, as highlighted by the histograms (*inset*).

in figure 10 contain histograms showing the number of stars (data: *grey*; model: *black*) along a cut through the subgiant branch (*thick line*). In figure 10c, the residual subgiant stars that are not reproduced by this old model (*inset*) suggest that at least 20% of the stars in the halo must be younger than 11.5 Gyr. We conclude that a purely old stellar population cannot explain the CMD of the M31 halo.

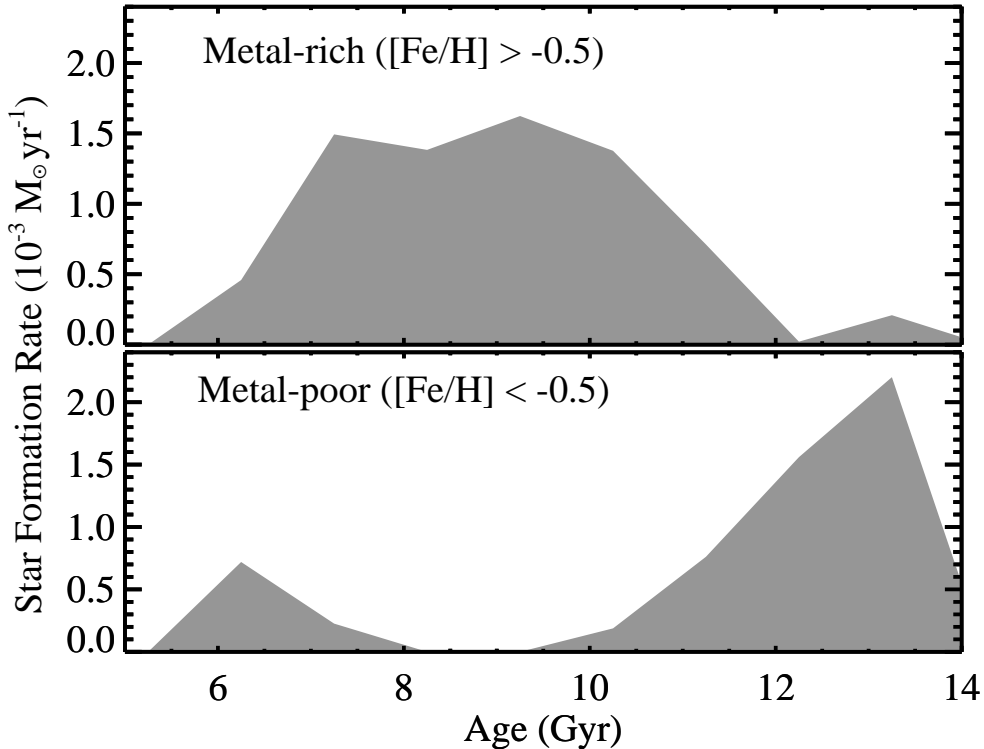


FIGURE 11. *Upper panel:* The star formation history of the metal-rich stars in the best model (figure 10d) obtained to date. The bulk of the metal-rich population is of intermediate age. *Lower panel:* The star formation history of the metal-poor stars in the best-fit model. Most of the metal-poor stars are old, but this model includes a small population of young metal-poor stars. Note that this star formation history is not unique; we can obtain a fit that is nearly as good as this fit, using two completely distinct population components (a purely old metal-poor population and a purely young metal-rich population). The detailed star formation history will be explored more fully in a future paper.

Next, we expanded the age range to 6–13.5 Gyr and repeated the fit (see figure 10d). The width of the red giant branch is now matched without a mismatch at the subgiant branch (*inset*). The best-fit model can be broadly characterized by a combination of two dominant populations (figure 11): 56% of the stars (*red*) are metal-rich ( $[\text{Fe}/\text{H}] > -0.5$ ) and of intermediate age (6–11 Gyr), while 30% of the stars (*blue*) are metal-poor ( $[\text{Fe}/\text{H}] < -0.5$ ) and old (11–13.5 Gyr). About half of this metal-rich population (i.e., 28% of the total population) is 6–8 Gyr old. Note that these models only illustrate, in a broad sense, the dominant populations present in the M31 halo. Other combinations of young metal-rich and old metal-poor stars are possible. For example, we produced a similar fit by combining two very distinct isochrone groups: one at 6–8 Gyr with  $[\text{Fe}/\text{H}] > -1$ , and one at 11.5–13.5 Gyr with  $[\text{Fe}/\text{H}] < -1$ . We are currently investigating detailed constraints on the star formation history.

## 5. Disk Contamination

Note that our halo field should be relatively free of stars moving in the stellar disk. Several estimates for the disk contribution at this distance range from 1–3%, even with a significant thick disk component (Holland et al. 1996 and references therein). On aver-

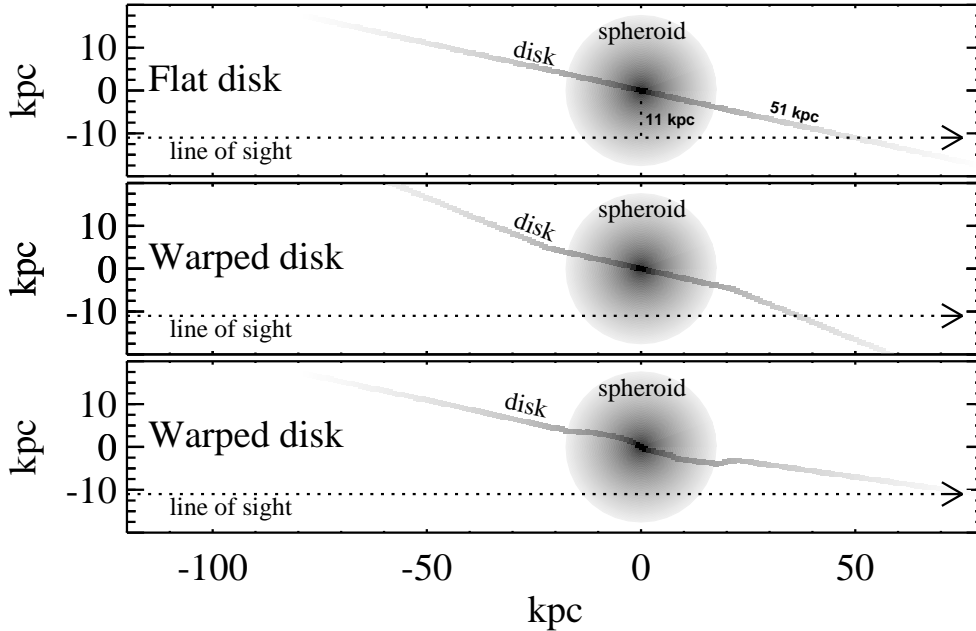


FIGURE 12. *Top panel:* A simple schematic showing the intersection of our sight-line with the Andromeda disk. The plane of the disk is inclined  $12.5^\circ$  with respect to our line of sight (de Vaucouleurs 1958), so that we are viewing the halo population at 11 kpc from the nucleus but the disk population at 51 kpc from the nucleus. The disk has an exponential scale length of 5.3 kpc (Walterbos & Kennicutt 1988). Note that the southeastern half of the disk is the side furthest from the observer (Iye & Richter 1985). *Middle panel:* The isophotes for Andromeda show evidence of a warp near 22 kpc on the major axis (Walterbos & Kennicutt 1987). Here, I insert a hypothetical  $10^\circ$  warp at 22 kpc on the minor axis, such that more of the disk population is moved into our sight-line. Our sight-line has effectively moved inward by about 2 scalelengths, increasing the disk population by a factor of 8. However, even with this large warp into our sight-line, the increase in the disk population would not explain the large population of intermediate-age stars we find in our field. *Bottom panel:* A more realistic depiction of the warp in the Andromeda disk, by interpolating the measurements of Braun (1991) along the minor axis. Early models of the warp (e.g., Henderson 1979) imply our sight-line would not intersect the disk at all, because of the increasing inclination at large distances from the nucleus. Later models (e.g., Braun 1991) indicate that the inclination varies from  $25^\circ$  close to the nucleus to  $10\text{--}15^\circ$  further out, as depicted here. The result is that our effective position within the disk is significantly beyond the 51 kpc shown in the top panel.

age, the plane of the disk is inclined from our sight-line by  $12.5^\circ$  (de Vaucouleurs 1958; figure 12, *top panel*), so we are observing halo stars 11 kpc from the nucleus but disk stars 51 kpc from the nucleus. A warp in the outer disk, if it angled the disk into our sight-line, would move the sight-line intersection with the disk inward, but even a large warp could not explain the number of young stars seen in our field. E.g., Walterbos & Kennicutt (1987) found a possible warping of the stellar disk at  $100'$  (22 kpc) on the southwest major axis. If we assume that the stellar disk along the southeast minor axis is warped such that the disk beyond 22 kpc is inclined by an additional  $10^\circ$  into our sight-line, this would move our effective disk position inward by about two scalelengths (figure 12, *middle panel*), increasing the disk population by a factor of 8 (i.e., the disk would contribute  $\approx 10\text{--}20\%$  of the total population in our field). However, we find that 56% of the stars in our field are metal-rich and of intermediate age, so this hypothetical increase in the disk contamination would not account for our surprisingly young popula-

tion. In reality, studies of the neutral gas kinematics (e.g., Braun 1991; Henderson 1979) find that the outer disk is actually viewed significantly closer to edge-on than the inner disk (figure 12, *bottom panel*), such that the warp in the disk would move our sight-line further out, beyond the intersection given by a flat disk. Finally, the fact that the metallicity distribution in our field is very similar to that twice as far out (Holland et al. 1996; Durrell, Harris, & Pritchett 2001) provides another strong indication that we are viewing a halo-dominated population.

## 6. Summary and Discussion

The CMD of the M31 halo is evidently inconsistent with a population composed solely of old (globular cluster age) stars; instead, it is dominated by a population of metal-rich intermediate-age stars. Although the high metallicity in the M31 halo is well-documented, the large age spread required to simultaneously reproduce the red giant branch, subgiant branch, and main sequence came to us as a surprise. Earlier studies of the red giant branch were insensitive to this age spread. For example, Durrell et al. (2001) were able to explain the metallicity distribution 20 kpc from the nucleus, with a simple chemical evolution model forming most of the stars at very early times (see also Côté et al. 2000). Although our field is relatively small in sky coverage, it appears representative; the metallicity in our field (Holland et al. 1996) agrees well with that much further out (Durrell et al. 2001), and there are no indications of substructure or tidal streams in the region we surveyed (Ferguson et al. 2002).

It seems unlikely that star formation in the halo proceeded for  $\sim 6$  Gyr from gas in situ; instead, the broad age dispersion in the halo is likely due to contamination from the disruption of satellites or of disk material into the halo during mergers. Indeed, our current analysis of the data cannot rule out the possibility that M31 and a nearly-equal-mass companion galaxy experienced a violent merger when the Universe was half its present age. If the 6–8 Gyr population in the halo represents the remnants of a disrupted satellite, the relatively high metallicity suggests that it must have been fairly massive. On the other hand, the stars could represent disruption of the M31 disk, either by a major collision when M31 was  $\sim 6$  Gyr old, or by repeated encounters with smaller satellites. The resulting halo would be a mix of the old metal-poor stars formed earliest in M31's halo, disk stars that formed prior to the merger(s) that were subsequently dispersed into the halo, stars formed during the merger(s), and the remnant populations of the disrupted satellite(s).

This work was done in collaboration with H.C. Ferguson, E. Smith (STScI), R.A. Kimble, A.V. Sweigart (NASA/GSFC), R.M. Rich, D. Reitzel (UCLA), A. Renzini (ESO), and D.A. Vandenberg (U. of Victoria). I am grateful to J. Harris (STScI) and P. Stetson (DAO) for respectively providing the StarFish and DAOPHOT-II codes and assistance in their use. Thanks to the members of the scheduling and operations teams at STScI (especially P. Royle, D. Taylor, and D. Soderblom) for their efforts in executing a large program during a busy HST cycle. Support for program 9453 was provided by NASA through a grant from the Space Telescope Science Institute, which is operated by the Association of Universities for Research in Astronomy, Inc., under NASA contract NAS 5-26555. The Digitized Sky Survey was produced at the Space Telescope Science Institute under U.S. Government grant NAG W-2166. The images of these surveys are based on photographic data obtained using the Oschin Schmidt Telescope on Palomar Mountain and the UK Schmidt Telescope. The plates were processed into the present compressed

digital form with the permission of these institutions. This research has made use of the SIMBAD database, operated at CDS, Strasbourg, France.

## REFERENCES

- AGUILAR, L., HUT, P., & OSTRIKER, J.P. 1988 On the evolution of globular cluster systems. I - Present characteristics and rate of destruction in our Galaxy. *ApJ* **335**, 720–747.
- BERTIN, E., & ARNOUITS, S. 1996 SExtractor: Software for source extraction. *A&AS* **117**, 393–404.
- BRAUN, R. 1991 The distribution and kinematics of neutral gas in M31. *ApJ* **372**, 54–66.
- BROWN, T.M., FERGUSON, H.C., SMITH, E., KIMBLE, R.A., SWEIGART, A.V., RENZINI, A., RICH, R.M., & VANDENBERG, D.A. 2003 Evidence of a Significant Intermediate-Age Population in the M31 Halo from Main-Sequence Photometry. *ApJ* **592**, L17–20.
- BULLOCK, J.S., KRAVTSOV, A.V., & WEINBERG, D.H. 2000 Reionization and the Abundance of Galactic Satellites. *ApJ* **539**, 517–521.
- CÔTÉ, P., MARZKE, R. O., WEST, M. J., & MINNITI, D. 2000 Evidence for the Hierarchical Formation of the Galactic Spheroid. *ApJ* **533**, 869–883.
- DE VAUCOULEURS, G. 1958 Photoelectric photometry of the Andromeda nebula in the UBV system. *ApJ* **128**, 465–488.
- DURRELL, P.R., HARRIS, W.E., & PRITCHET, C.J. 2001 Photometry and the Metallicity Distribution of the Outer Halo of M31. *AJ* **121**, 2557–2571.
- EGGEN, O.J., LYNDEN-BELL, D., & SANDAGE, A.R. 1962 Evidence from the motions of old stars that the Galaxy collapsed. *ApJ* **136**, 748–766.
- FERGUSON, A.M.N., IRWIN, M.J., IBATA, R.A., LEWIS, G.F., & TANVIR, N.R. 2002 Evidence for Stellar Substructure in the Halo and Outer Disk of M31. *AJ* **124**, 1452–1463
- FORD, H.C., ET AL. 1998 Advanced camera for the Hubble Space Telescope. *SPIE* **3356**, 234–248.
- FREEDMAN, W.L., & MADORE, B.F. 1990 An empirical test for the metallicity sensitivity of the Cepheid period-luminosity relation. *ApJ* **365**, 186–194.
- HARRIS, W.E. 1996 A Catalog of Parameters for Globular Clusters in the Milky Way. *AJ* **112**, 1487–1488.
- HARRIS, J., & ZARITSKY, D. 2001 A Method for Determining the Star Formation History of a Mixed Stellar Population. *ApJS* **136**, 25–40.
- HEITSCH, E., & RICHTLER, T. 1999 The metal-rich globular clusters of the Milky Way. *A&A* **347**, 455–472.
- HENDERSON, A.P. 1979 A Model for the Orientation of M31. *A&A* **75**, 311–315.
- HOLLAND, S., FAHLMAN, G.G., & RICHER, H.B. 1996 Deep HST V- and I-Band Observations of the Halo of M31: Evidence for Multiple Stellar Populations. *AJ* **112**, 1035–1045.
- HOLLAND, S., FAHLMAN, G.G., & RICHER, H.B. 1996 Deep HST V- and I-Band Observations of Two Globular Clusters in the Halo of M31. *AJ* **114**, 1488–1507.
- HUCHRA, J.P., BRODIE, J.P., & KENT, S.M. 1991 Extragalactic globular clusters. II – The M31 globular cluster system. *ApJ* **370**, 495–504.
- IBATA, R.A., GILMORE, G., & IRWIN M.J. 1994 A Dwarf Satellite Galaxy in Sagittarius. *Nature* **370**, 194–196.
- IBATA, R., IRWIN, M., LEWIS, G., FERGUSON, A.M.N., & TANVIR, N. 2001 A giant stream of metal-rich stars in the halo of the galaxy M31. *Nature* **412**, 49–52.
- IBEN, I., & RENZINI, A. 1984 Single star evolution I. Massive stars and early evolution of low and intermediate mass stars. *PhR* **105**, 329–406.
- IYE, M., & RICHTER, O.-G. 1985 Reddening of globular clusters in M 31. *A&A* **144**, 471–478.
- KLYPIN, A., ZHAO, H.S., & SOMERVILLE, R.S. 2002  $\Lambda$ CDM-based Models for the Milky Way and M31. I. Dynamical Models. *ApJ* **573**, 597–613.
- KRIST, J. 1995 Simulation of HST PSFs using Tiny Tim. In *Astronomical Data Analysis Software and Systems IV* (ed. R.A. Shaw, H.E. Payne, & J.J.E. Hayes). ASP Conference Series, vol. 77, pp. 349–352. ASP.
- LARSON, R.B. 1969 A model for the formation of a spherical galaxy. *MNRAS* **145**, 405–422.

- LEJEUNE, T., CUISINIER, F., & BUSER, R. 1997 Standard stellar library for evolutionary synthesis. I. Calibration of theoretical spectra. *A&AS* **125**, 229–246.
- MAJEWSKI, S.R., OSTHEIMER, J.C., KUNKEL, W.E., & PATTERSON, R.J. 2000 Exploring Halo Substructure with Giant Stars. I. Survey Description and Calibration of the Photometric Search Technique. *AJ* **120**, 2550–2568.
- MCCONNACHIE, A.W., IRWIN, M.J., IBATA, R.A., FERGUSON, A.M.N., LEWIS, G.F., & TANVIR, N. 2003 The three dimensional structure of the giant stellar stream in Andromeda. *MNRAS*, in press. astro-ph/0305160.
- MOMANY, Y., ET AL. 2003 V, J, H and K imaging of the metal rich globular cluster NGC 6528. Reddening, metallicity, and distance based on cleaned colour-magnitude diagrams. *A&A* **402**, 607–616.
- MOORE, B., GHIGNA, S., GOVERNATO, F., LAKE, G., QUINN, T., STADEL, J., & TOZZI, P. Dark Matter Substructure within Galactic Halos. *ApJ* **524**, L19–L22.
- MORRISON, H.L., MATEO, M., OLSZEWSKI, E.W., HARDING, P., DOHM-PALMER, R.C., FREEMAN, K.C., NORRIS, J.E., & MORITA, M. 2000 Mapping the Galactic Halo. I. The “Spaghetti” Survey. *AJ* **119**, 2254–2273.
- MOULD, J., & KRISTIAN, J. 1986 The stellar population in the halos of M31 and M33. *ApJ* **305**, 591–599.
- RENZINI, A., ET AL. 1996 The White Dwarf Distance to the Globular Cluster NGC 6752 (and Its Age) with the Hubble Space Telescope. *ApJ* **465**, L23–L26.
- RYAN, S.G., & NORRIS, J.E. 1991 Subdwarf Studies. III. The Halo Metallicity Distribution. *AJ* **101**, 1865–1878.
- SANDAGE, A. 1982 The Oosterhoff period groups and the age of globular clusters. III - The age of the globular cluster system. *ApJ* **242**, 553–581.
- SARGENT, W.L.W., KOWAL, C.T., HARTWICK, F.D.A., VAN DEN BERGH, S. 1977 Search for globular clusters in M31. I - The disk and the minor axis *AJ* **82**, 947–953
- SEARLE, L., & ZINN 1978 Compositions of halo clusters and the formation of the galactic halo. *ApJ* **225**, 357–379.
- SCHLEGEL, D.J., FINKBEINER, D.P., & DAVIS, M. 1998 Maps of Dust Infrared Emission for Use in Estimation of Reddening and Cosmic Microwave Background Radiation Foregrounds. *ApJ* **500**, 525–553.
- STETSON, P. 1987 DAOPHOT - A computer program for crowded-field stellar photometry *PASP* **99**, 191–222.
- VAN DEN BERGH, S. 1992 The luminosity function of the Local Group. *A&A* **264**, 75–76.
- VANDENBERG, D.A. 2000 Models for Old, Metal-Poor Stars with Enhanced  $\alpha$ -Element Abundances. II. Their Implications for the Ages of the Galaxy’s Globular Clusters and Field Halo Stars. *ApJS* **129**, 315–352.
- VANDENBERG, D.A., BOLTE, M., & STETSON, P.B. 1990 Measuring age differences among globular clusters having similar metallicities - A new method and first results. *AJ* **100**, 445–468.
- VANDENBERG, D.A., & CLEM, J.L. 2003 Empirically Constrained Color-Temperature Relations. I. BV(RI)<sub>C</sub>. *AJ* **126**, in press.
- VANDENBERG, D. A., RICHARD, O., MICHAUD, G., & RICHER, J. 2002 Models of Metal-poor Stars with Gravitational Settling and Radiative Accelerations. II. The Age of the Oldest Stars. *ApJ* **571**, 487–500.
- WALTERBOS, R.A.M., & KENNICUTT, R.C., JR. 1987 Multi-color photographic surface photometry of the Andromeda galaxy. *A&AS* **69**, 311–322.
- WALTERBOS, R.A.M., & KENNICUTT, R.C., JR. 1988 An optical study of stars and dust in the Andromeda galaxy. *A&A* **198**, 61–86.
- WHITE, S.D.M., & FRENK, C.S. 1991 Galaxy formation through hierarchical clustering. *ApJ* **379**, 52–79.
- WILLIAMS, R.E., ET AL. 1996 The Hubble Deep Field: Observations, Data Reduction, and Galaxy Photometry. *AJ* **112**, 1335–1389.
- ZOCCALI, M., ET AL. The White Dwarf Distance to the Globular Cluster 47 Tucanae and its Age. *ApJ* **553**, 733–743.